IOP Publishing Nanotechnology

Nanotechnology **21** (2010) 175301 (7pp) doi:10.1088/0957-4484/21/17/175301

The fabrication of ordered arrays of exchange biased Ni/FeF_2 nanostructures

M Kovylina[1], M Erekhinsky[2], R Morales[3], I K Schuller[2], A Labarta[1] and X Batlle[1]

[1] Departament de Física Fonamental and Institut de Nanociència i Nanotecnologia, Universitat de Barcelona, 08028 Barcelona, Catalonia, Spain
[2] Physics Department, University of California San Diego, La Jolla, CA 92093, USA
[3] Departamento de Química Física, University of the Basque Country, Leioa 48940, Vizcaya, Spain

E-mail: miroslavna@ffn.ub.es (M Kovylina) and xavierbatlle@ub.edu

Received 26 January 2010, in final form 10 March 2010
Published 1 April 2010
Online at stacks.iop.org/Nano/21/175301

Abstract

The fabrication of ordered arrays of exchange biased Ni/FeF_2 nanostructures by focused ion beam lithography is reported. High quality nano-elements, with controlled removal depth and no significant re-deposition, were carved using small ion beam currents (30 pA), moderate dwell times (1 μs) and repeated passages over the same area. Two types of nanostructures were fabricated: square arrays of circular dots with diameters from 125 $\pm$ 8 to 500 $\pm$ 12 nm and periodicities ranging from 200 $\pm$ 8 to 1000 $\pm$ 12 nm, and square arrays of square antidots (207 $\pm$ 8 nm in edge length) with periodicities ranging from 300 $\pm$ 8 to 1200 $\pm$ 12 nm. The arrays were characterized using scanning ion and electron microscopy, and atomic force microscopy. The effect of the patterning on the exchange bias field (i.e., the shift in the hysteresis loop of ferromagnetic Ni due to proximity to antiferromagnetic FeF_2) was studied using magneto-transport measurements. These high quality nanostructures offer a unique method to address some of the open questions regarding the microscopic origin of exchange bias. This is not only of major relevance in the fabrication and miniaturization of magnetic devices but it is also one of the important proximity phenomena in nanoscience and materials science.

(Some figures in this article are in colour only in the electronic version)

1. Introduction

Nanostructured materials have attracted much attention over the recent years, as they provide the building blocks for nanoscience and nanotechnology [1–4]. Research on nanostructures has driven the sample physical size towards ever-smaller dimensions. Nanostructures have novel and enhanced properties over their bulk counterparts due to the interplay among finite-size, surface and proximity effects [1–4]. Fundamentally, novel properties emerge as the sample size becomes comparable to or smaller than certain characteristic length scales, such as the spin diffusion length, carrier mean free path, magnetic domain wall width or superconducting coherence length. While the electrons are confined in small structures, an appreciable fraction of their wavefunction resides outside the physical extension of the nanostructure, such that 'proximity effects' become more important with decreasing size. Recent progress has made magnetic nanostructures a particularly interesting class of materials for both scientific and technological explorations [5–7]. For example, studies on interlayer coupling, giant magnetoresistance, tunneling and colossal magnetoresistances, exchange bias, half-metallic ferromagnets (FM) and spin injection have led to the exciting possibility of using the electron spin for information processes, or *spintronics* [8, 9]. Thus, transport of charge and spin in nanostructured magnetic materials is one of the most active research fields [1, 2, 8–12].

Technologically, the device miniaturization trend has led, most visibly, to the explosive growth of the magnetic recording density. Magnetic nanostructures are also relevant in applications such as magnetic random access memories, patterned recording media, magnetic switches or magnetic sensors. Such demands call for advanced sample growth

and patterning techniques to achieve nanometer-scale feature sizes, beyond the limits of conventional photolithography. In practice, it is equally challenging to characterize such small nanostructures. Consequently, it is highly desirable not only to fabricate ultra-fine nanostructures, but also to fabricate ordered arrays of these nanostructures [4, 13]. Within this framework, nanofabrication by ion/electron beam lithography and self-organized templates is being explored intensively [4]. In particular, ion beam lithography using focused ion beams (FIBs) has proven very successful in the fabrication of sub-micron nanostructures [14, 15]. Ordered arrays of magnetic nanostructures are particularly interesting, as one can probe both the individual and collective behavior of the elements in a well defined and reproducible fashion.

Proximity effects become very relevant for nanostructures that are in contact with other materials. While they have been investigated for many years in the field of superconductivity, the existence of similar effects in magnetism is the object of active research. Moreover, the induced magnetic fields also extend a considerable distance outside the nanostructure. Thus, the interplay between size confinement and proximity effects becomes particularly interesting. One outstanding example of a proximity effect in magnetic materials is exchange bias (EB) in FM/antiferromagnetic (AF) heterostructures [16]. EB is usually described as an additional unidirectional anisotropy induced by the AF into the FM via exchange coupling at the interface. The FM 'feels' an additional field to the applied magnetic field which produces a shift in the hysteresis loop, the so-called exchange bias field. Despite the facts that it has been studied extensively for years—it was discovered in Co–CoO nanoparticles back in the 1950s [17, 18]—and it is of great utility in read heads, magnetic random access memories and magnetic devices, the comprehensive explanation for EB still remains a challenge [16, 19–21]. The variability of results in the literature is mainly due to the variety of parameters which affect the microstructure of the materials. Among others, the relative size of the FM and AF magnetic domains, the FM–AF interface structure and roughness, and the actual location of the pinned, uncompensated AF spins that create the exchange field on the FM seem to play a crucial role in the coupling mechanism [22–27].

The study of nanostructured AF/FM heterostructures with nanoscopic feature sizes is useful for probing the role of the domain size and morphology, and the effect of lateral confinement on both the EB phenomena and magnetization reversal mechanisms, when the distances and/or sizes of the nano-elements are comparable to FM and/or AF domain lengths [19, 28]. We have recently shown that the nanostructure may modify the number of pinned, uncompensated spins in the AF that are responsible for the exchange field acting on the FM [29]. However, the large number of controversial experimental data [19, 21] suggests that further advance in the understanding of this phenomenon should start with the fabrication of high quality and reproducibility model samples.

In this paper, focused ion beam lithography (FIB) using Ga^+ ions was chosen as the optimum fabrication technique for EB studies in nanostructures due to (i) its nanoscale resolution capabilities, (ii) the reasonable fabrication time-to-structure quality ratio, (iii) the high reproducibility, (iv) the almost direct pattern-to-object shape conversion and (v) the fine control on the removal depth. In addition, since photo-resists are not used, issues regarding chemical residues at the FM/AF or AF/substrate interfaces are avoided. Moreover, the dependence of the nano-element shape on the FIB dose can be controlled more easily than in electron beam lithography. The latter is highly dependent, for example, on the resist quality, homogeneity and thickness. Two types of ordered arrays were prepared: circular dots and square antidots. Both of them were fabricated from Ni (50 nm)/FeF_2 (70 nm) FM/AF heterostructures, grown by electron beam evaporation on epitaxial and untwinned (110) FeF_2. We show that there was no significant degradation of the magnetic and transport properties after patterning.

Much work had been performed previously on un-patterned FM/FeF_2 heterostructures (FM = Fe, Ni, ...), since FeF_2 is an AF (Néel temperature, $T_N = 78.4$ K) that may be grown epitaxially, leading to large crystallographic domains. The control of the interface roughness enabled some of us to show that exchange bias depends critically on the relative FM and AF domain size [22, 23, 30], i.e., on the lateral characteristic length scales on the two sides of the interface. While there are uncompensated pinned (frozen) AF spins at the interface and in the bulk, there are also uncompensated unpinned (free) AF spins at the interface [24–27]. The precise role these play in the EB is not well understood.

The FIB-patterned Ni/FeF_2 nanostructures in this paper are thus model systems for studies of EB since the nano-element size and periodicity (center-to-center distance) can be chosen to be close to typical domain wall widths in 3d FMs (up to a hundred nanometers) [23] and AF domains (larger than hundreds of nanometers) [22, 28].

2. Experimental details

Ni/FeF_2 heterostructures were deposited by electron beam evaporation onto (110) MgF_2 single-crystal substrates of 70 nm of FeF_2 at 300 °C and 50–70 nm of Ni and 4 nm of Al (to prevent oxidation) at 150 °C, all of them at 1 Å s^{-1} rate. In order to ensure the good quality of the FM/AF interface, all layers were evaporated without breaking vacuum. X-ray diffraction showed that FeF_2 grew epitaxial and untwinned in the (110) orientation. In order to obtain a variety of identical samples, the layers were deposited onto a 1 cm^2 (110) MgF_2 substrate, in the case of dots (figure 1(a)) using a shadow mask in the form of square areas of 400 μm in length (figure 2(a)), and in the case of antidots (figure 1(b)) patterning the substrate by photolithography in the form of stripes 10 μm wide and 90 μm long (figure 2(b)) with all the electrodes required to measure the four probe magneto-transport in an external magnetic field (figure 2(b)). Both types of samples were always patterned through the whole depth of the Ni/FeF_2 heterostructure (figures 1(a) and (b)).

One of the problems occurring during FIB pattering is the electrical charging of the nanostructure, which determines to a great extent its resolution and reproducibility. Therefore, the connection of the samples to the sample-holder ground

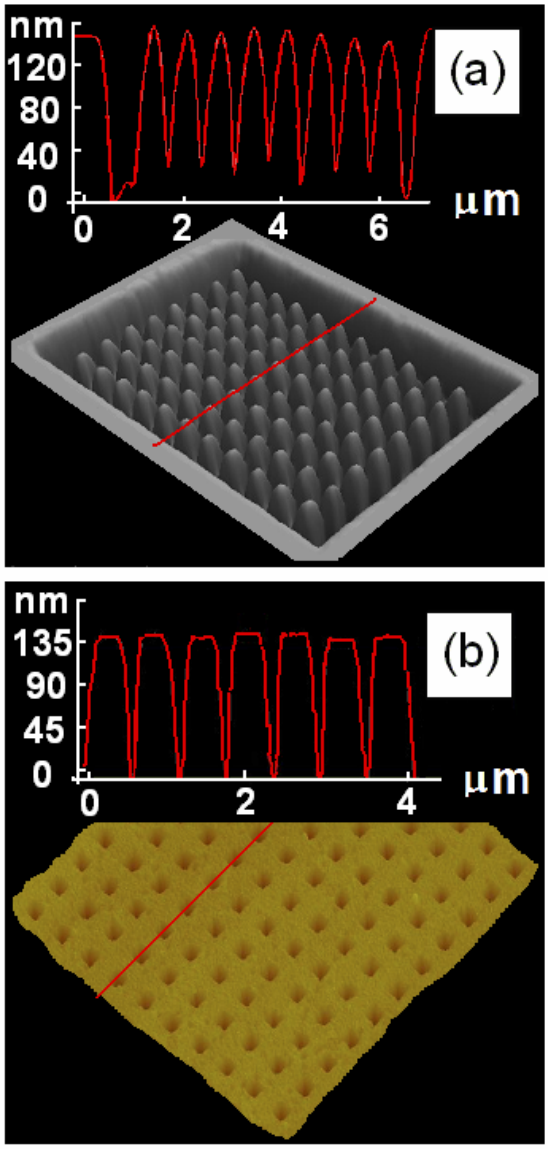

Figure 1. AFM images of (a) circular dots (300/600 nm in diameter/periodicity) and (b) square antidots (200 nm in edge length) with antidot areal density AD = 0.24.

is a critical issue. In the case of dots (figure 2(a)), an additional 4 nm Au layer was deposited by dc sputtering, providing a metallic equipotential surface. In the case of antidots, photolithography and dc-sputtering deposition were used to pattern Au pads (70 nm thick) that contact the different Ni/FeF_2 stripes (figure 2(b)). The connection of the sample to the sample-holder ground was provided by a sticky adhesive sheet. We found that the resolution and reproducibility of the nanostructure were higher if a copper conductive adhesive sheet was used instead of a carbon one which blurred the definition of the structure. Au pads were also used as contacts to measure the magneto-transport properties (figure 2(b)).

3. Results and discussion

Prior to the array fabrication (figure 1), we performed a calibration of the ion beam, devoting special attention to

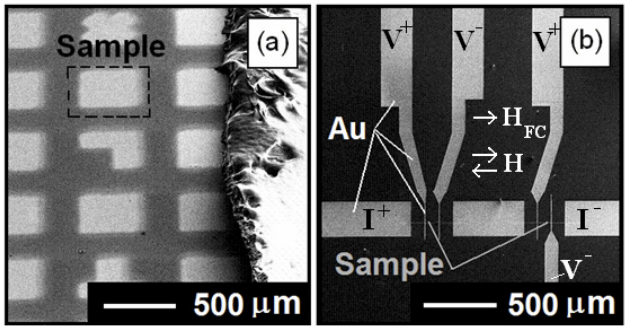

Figure 2. SEM images of (a) 400 μm × 400 μm squares for dot patterning; (b) 10 μm × 90 μm stripes for antidot fabrication and gold electrodes for magneto-transport measurements. The arrows indicate the measuring and cooling field directions for the parallel configuration.

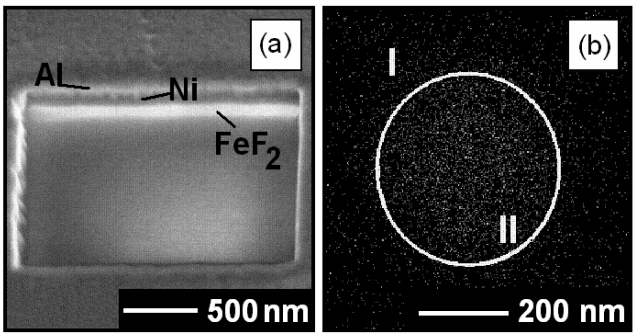

Figure 3. (a) SEM image showing an antidot depth profile, where the three layers (Al, Ni and FeF_2) can be easily distinguished; (b) EDX 2D map of the Ga^+ implantation (bright spots): I—outside the antidot area; II—inside the antidot area.

the removal depth, Ga^+ implantation and quality of the shape of the nano-element. The latter included the profile perpendicularity of the carved element with respect to the sample free surface, re-deposition, and the dot circularity and antidot squareness. The profile perpendicularity has the largest impact, since it was important to fabricate nanostructures with identical lateral FM and AF domain confinement. This must also include the Al and Au protecting and ground layers, respectively. To control the removal depth, three techniques were used: *in situ* scanning ion/electron microscopy (SIM and SEM, respectively) during fabrication (figure 3(a)) and atomic force microscopy (AFM) and SEM *ex situ* after patterning (figure 1). SIM is much more sensitive than SEM to the chemistry and microtexture of the layers, which allowed detection of when the Ga^+ ion beam switched between different layers. SIM was also used for the ion beam calibration, alignment and verification of the spot size. Although SEM provides less information about the layer being carved, it is much less destructive than SIM and it allows characterization of the nanostructure size and shape. In figure 3(a), Al, Ni and FeF_2 layers can be easily distinguished, also showing the lateral section, with a lateral resolution better than 6 nm for an antidot of about 2 μm in length.

After ion beam calibration, the three main ion beam parameters were fine-tuned: (i) the ion beam current, to adjust

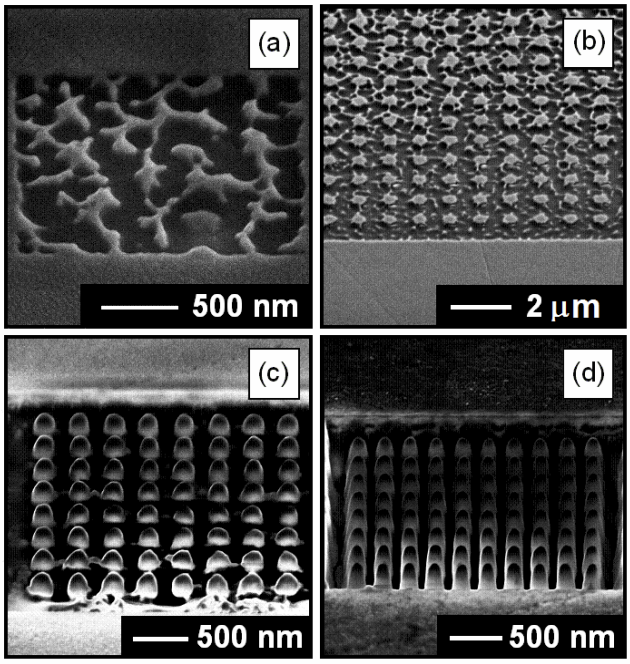

Figure 4. Ion beam current (pA) tuning: (a) 200; (b) 100; (c) 80; (d) 50. Dwell time (2 μs) and repetition number (one passage) are fixed.

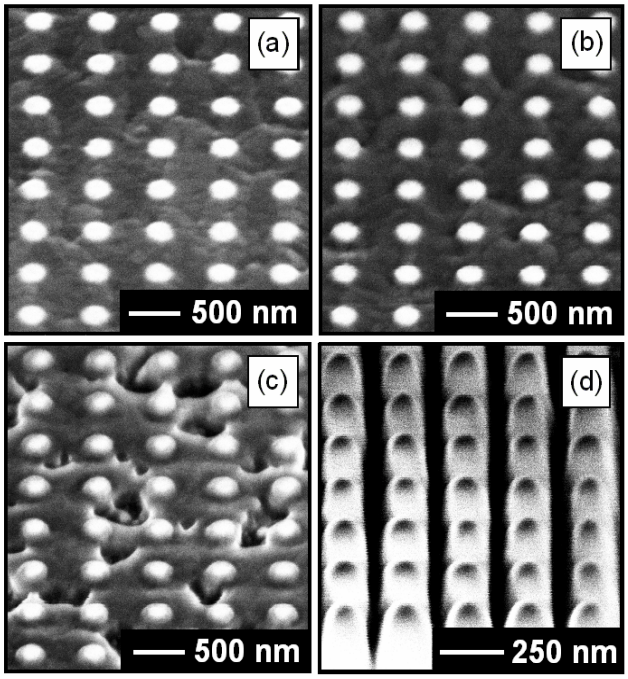

Figure 5. Dwell time (μs) tuning: (a) 0.1; (b) 0.5; (c) 1; (d) 2. Ion beam current (50 pA) and repetition number (one passage) are fixed.

the removal rate and total patterning time; (ii) the dwell time, i.e. the time for which the beam spot stays over one specific area of the sample, to set the milling depth and element shape; and (iii) the repetition number, i.e. the number of beam scans over the same area. Ultimately, these three parameters fix directly the beam dose. However, our studies showed that the quality of the nanostructure depends on a delicate interplay among all them and that it is much better to tune one parameter at a time. We also observed that the resolution improves at a combined lower current and larger dwell time. Hence, the first parameter to be tuned was the ion beam current, while the other two were kept fixed.

Figure 4 shows that the fabrication of circular dots of about 200 nm in diameter required an ion current smaller than 80 pA (figure 4(d)), because higher ones produce either total element destruction (figure 4(a)) above 200 pA or inhomogeneous removal (figures 4(b) and (c)) above 100 pA. Once the ion beam current was optimized and fixed at 50 pA, the dwell time was tuned. While short dwell times (above 0.1 μs) cause either scanty (figure 5(a)) or incomplete (figures 5(b) and (c)) material removal for 0.5 and 1 μs, respectively, we chose to over-expose the samples for 2 μs to ensure that both the FM and AF layers were carved out completely (figure 5(d)).

If the sample thermal drift and equipment vibrations are low during the whole fabrication process the quality of the nanostructure can be enhanced by shortening the dwell time and increasing the repetition number. An insufficient removal depth for 5–10 repetitions (figures 6(a) and (b), respectively) gives a highly perpendicular profile if the repetitions are increased to 20 and 40 (figures 6(c) and (d), respectively). Repeated passage over the same area produced insignificant rounding of the top of the nano-elements (figure 6(c)) and

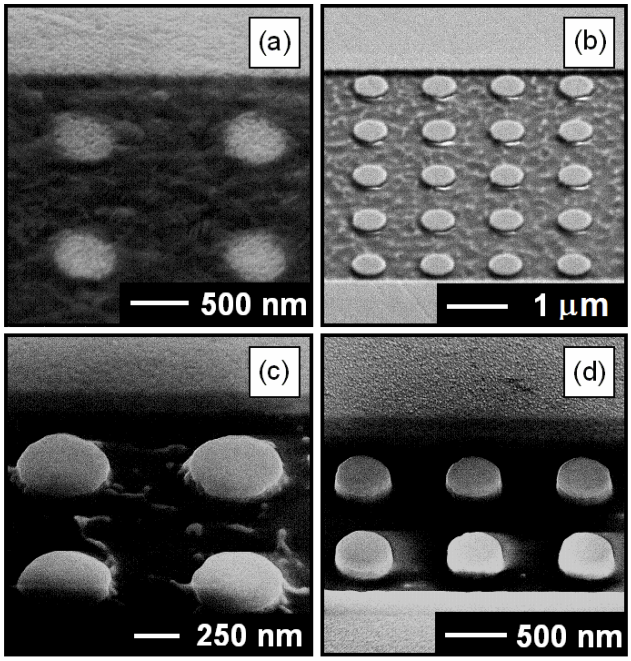

Figure 6. Repetition number tuning (number of passages): (a) 5; (b) 10; (c) 20; (d) 40. Ion beam current (50 pA) and dwell time (0.1 μs) are fixed.

material re-deposition (figure 6(d)), in contrast to a single passage, which requires higher ion beam doses to increase removal depth (figure 4(d)).

Another crucial issue in FIB fabrication is Ga^+ implantation. In order to characterize this effect, 20 nm Ni and 4 nm Al bilayers were deposited by dc sputtering on a silicon nitride membrane. Circular antidot arrays with different

Table 1. Relative percentage of implanted Ga^+ (%) for two antidot densities, AD = 0.17 and AD = 0.25, for three ion beam doses (1×, 2×, 5×; 1× corresponds to the dose required to etch completely a Si reference layer of 30 nm in thickness) and for two zones in the samples, I—outside, II—inside the antidot, as shown in figure 3(b). Error bars in Ga^+ concentration are about ±1%.

	Zone I, Ga^+ (%)		Zone II, Ga^+ (%)	
FIB dose	AD = 0.17	AD = 0.25	AD = 0.17	AD = 0.25
1×	1.3	1.1	7	7
2×	1.1	1.1	12	11
5×	3	2	20	20

antidot areal densities (ADs)—i.e., the ratio between the area of the patterned region and the total area of the sample—were patterned. Three different ion beam doses were used (table 1): the first one (1×) corresponds to the dose required to completely etch a 30 nm thick Si layer, while the second (2×) and the third ones (5×) were twice and five times the size of the first one, respectively.

Energy dispersive x-ray spectroscopy (EDX) analysis was performed, yielding the Ni, Al and Ga^+ element maps (figure 3(b)). We defined the relative percentage of implanted Ga^+ (table 1) as the ratio between the number of counts for Ga^+ and the sum of counts for Ni, Al and Ga^+. The analysis of element maps (table 1) demonstrated that for AD = 0.17 and 0.25 the percentage of implanted Ga^+ for the neighboring area outside the antidot does not exceed 3% for the maximum dose. Inside the antidot, the Ga^+ implantation was higher, amounting to 20% as the ion beam dose increases. In the case of the Ni/FeF_2 samples, as the material removal process stops right after reaching the substrate, most of the Ga^+ implantation takes place in the MgF_2 substrate and it almost has no effect on the magnetic properties of the FM/AF nano-elements. The fact that even for the highest ion beam dose and larger AD the percentage of implanted Ga^+ outside the antidots is low implies that the EB should not change significantly with patterning (see below).

Once the ion beam calibration and parameter tuning was performed, ordered arrays of dots and antidots were fabricated using 30 pA ion current and 1 μs dwell time. The repetition number was adjusted to remove all layers down to the substrate. The AFM images (figure 1) proved that the removal depth is sufficient to carve the nanostructures throughout the FM and AF layers for both types of samples. The rounded tops of the dots (figure 1(a)) and the poor perpendicularity of the dot and antidot sides (figures 1(a) and (b)) are artifacts of the AFM technique, as found in the SEM images of figures 4–6. AFM did not produce a good structural image for the typical depths (124–150 nm), because of the convolution of the real image with the tip shape. A variety of square arrays of circular dots with diameter from 125 ± 8 nm to 500 ± 12 nm and square arrays of square antidots (207 ± 8 nm in edge length) were fabricated, with AD ranging from 0.07 to 0.51 and side-to-side distance from 1000 ± 12 nm to 100 ± 8 nm, respectively.

These patterned antidot arrays combined with transport measurements gave us a deeper insight into the EB properties of the system. Magnetoresistance (MR) is an excellent technique to study the EB in the present nanostructures. First,

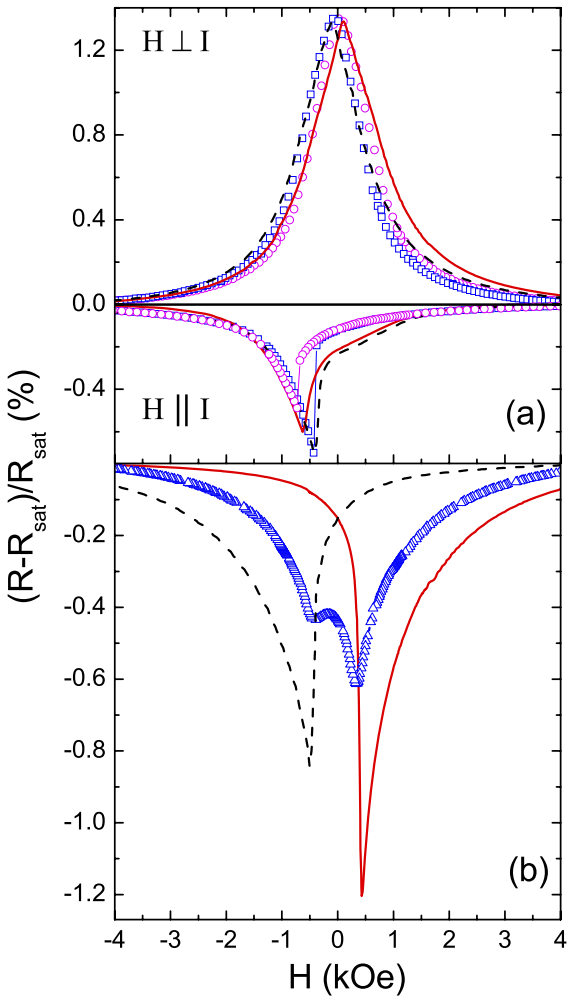

Figure 7. Example of magnetoresistance, MR (defined as $(R–R_{sat})/R_{sat}$, where R is the resistance at a field H, and R_{sat} is the resistance at the saturation field), as a function of magnetic field, H, measured at 4.2 K after a field cooling process (FC) under the following conditions: (a) transverse ($H \perp I$; I—electrical current injected) and parallel ($H \parallel I$) geometry for FC = 0.7 T, for the un-patterned samples (AD = 0)/antidot density AD = 0.06, where the decreasing (pink circles/red solid line) and increasing (blue squares/black dashed line) field branches are presented; (b) parallel geometry for AD = 0.06, after a field cooling process at the following cooling fields: FC = 0.019 (black dashed line), 0.8 (blue open triangles), 2 T (red solid line).

it allows measurement of a small patterned area, being very sensitive to local magnetization, and it provides the loop asymmetry, which is related to the reversal mode. Second, and most important, it is controlled only by the FM Ni through which the current flows, since FeF_2 is an insulator. The resistance of both Ni/FeF_2 un-patterned heterostructures and samples containing antidots was measured in a magnetic field, using a standard four probe technique in the temperature range 4.2–300 K up to 50 kOe (figure 7).

Based on the bulk structure, the ideal (110) FeF_2 interfacial plane is assumed to have compensated spins, oriented in plane and with the easy axis along the [001] direction of the crystal. Magnetization measurements also showed that the polycrystalline Ni layer displayed a growth-

induced uniaxial anisotropy along the [001] FeF_2 easy axis [22]. The injected electrical current I (figure 2(b)) was always applied along the (110) plane and parallel to the [001] FeF_2 (and Ni) easy axis. The magnetic field was applied in plane, either parallel (the case for parallel geometry is shown in figure 2(b)) or transverse (transverse geometry: measuring and cooling field directions are perpendicular to those shown in figure 2(b)) to the injected electrical current. The resistance was measured at various cooling fields (from 100 Oe to 50 kOe). The measuring field, H, was applied parallel to the cooling field H_{FC}.

Figure 7(a) shows representative R–H curves both in the transverse and parallel geometry. Deeper knowledge regarding the importance of interfacial properties for EB may be gained by comparing the MR behavior before and after patterning. First, the peak depth in both the parallel and transverse configurations, and the peak position in the parallel configuration, are exactly the same before and after patterning, reflecting that there is no significant degradation of either the magnetic, transport or EB properties with patterning. Second, before and after fabrication the MR is positive for the transverse configuration (showing no loop shift), and negative for the parallel one (showing loop shift), which implies that there is no change in the easy axis of the EB domains. Third, the differences in the curve shapes before and after patterning might be related to a modification in the magnetization reversal associated with confinement of the domains.

Three types of behavior were observed in the parallel geometry for all patterned samples as a function of the cooling field (figure 7(b)): for small cooling fields, R–H curves exhibit negatively (along the H axis) shifted peaks at the coercive field (negative EB) [17–21], while for large cooling fields the shift was positive (positive EB) [31] (figure 7(b)). At intermediate cooling fields, two peaks were observed (one shifted to negative; the other to positive fields) whose relative height and area depended on the cooling field, resulting in double hysteresis loops (DHLs) [22, 23, 29]. In all cases, the absolute value of the exchange bias field, i.e., the loop shift, was almost independent of the cooling field, at a given AD (i.e., the peak positions appear at the same absolute value of the magnetic field for all three cases in figure 7(b)). All of the above suggests that the AF domain size is comparable to or larger than the FM domain size, so each FM domain couples mostly to a single AF domain with a particular direction of the EB [22, 23]. Therefore, for small and large cooling fields only one EB direction arises, while two directions appear at intermediate cooling fields. In this case, the samples split magnetically into two equivalent subsystems with opposite direction of the EB, being these two subsystems at the origin of the DHL. The relative height and area of the peaks in the R–H curves depend on the total amounts of each of the two subsystems. These results match well previous results in FM/AF un-patterned heterostructures [22, 23]. This confirms that patterned nanostructures maintain the local, non-averaging nature of the EB, related to the key role of the relative lateral characteristic length scales on the two sides of the interface (relative size of FM and AF domains). This is a nice illustration of the proximity effect observed when two dissimilar materials are in intimate contact and the properties of one affects those of the other.

4. Conclusions

Ordered arrays of exchange biased Ni/FeF_2 nanostructures have been successfully fabricated by FIB. Extensive studies revealed that the best control may be achieved using the lowest possible ion beam current (about 30 pA), moderate dwell time (about 1–2 μs) and repeated passage of the ion beam over the same area, the latter minimizing re-deposition and over-dosing effects. Square arrays of square antidots were chosen to study the influence of lateral confinement on the exchange bias field and on FM and AF domains. Ion/electron scanning microscopy, energy dispersive x-ray spectroscopy, atomic force microscopy and magneto-transport measurements showed that FIB using low ion beam dosages is a convenient technique for the fabrication of high quality EB nanostructures. All in all, these high quality nanostructures offer a unique method to address the open questions regarding the microscopic origin of the exchange bias. These studies are not only relevant for basic research in solid state physics but also provide the means to improve storage, spintronic and sensor devices which rely on nanostructured magnetism.

Acknowledgments

The financial support of the Spanish MICINN (MAT2006-03999, MAT2009-08667 and PhD grant of MK), Catalan DURSI (2009SGR856), University of Barcelona (International Cooperation) and the US Air Force Office for Scientific Research and Department of Energy are recognized. RM also acknowledges sponsorship from Ikerbasque Foundation, European Marie Curie OIF and Spanish Grant Nos. MICINN FIS2008-06249 and FICYTIB08-106. The authors are indebted to J E Villegas (CNRS-Thales, Université Paris Sud, France) for critical discussion of the transport data and to the Nanotechnology Platform of the Barcelona Science Park of the University of Barcelona for assistance during FIB fabrication.

References

[1] For a review see Batlle X and Labarta A 2002 *J. Phys. D: Appl. Phys.* **35** R15
[2] Fullerton E E and Schuller I K 2007 *ACS Nano* **1** 384
[3] For a review see Bader S D 2006 *Rev. Mod. Phys.* **78** 1
[4] For a review see Martín J I, Nogués J, Liu K, Vicent J L and Schuller I K 2003 *J. Magn. Magn. Mater.* **256** 449 and references therein
[5] Wolf S and Treger D 2000 *IEEE Trans. Magn.* **36** 2748
[6] Kools J C S 1996 *IEEE Trans. Magn.* **32** 3165
[7] Parkin S S P, Jiang X, Kaiser C, Panchula A, Roche K and Samant M 2003 *Proc. IEEE* **91** 661
[8] Prinz G A 1998 *Science* **282** 1660
[9] Akerman J 2005 *Science* **308** 508
[10] Baibich M N *et al* 1988 *Phys. Rev. Lett.* **61** 2472
[11] Binasch G, Grünberg P, Saurenbach F and Zinn W 1989 *Phys. Rev.* B **39** 4828
[12] For a review see Gregg J F, Petej I, Jouguelet E and Dennis C 2002 *J. Phys. D: Appl. Phys.* **35** R121
[13] Ross C A 2001 *Annu. Rev. Mater. Res.* **31** 203

[14] Giannuzzi L A and Stevie F A 2005 *Introduction to Focused Ion Beams: Instrumentation, Theory, Techniques and Practice* (New York: Springer)
[15] Orloff J, Utlaut M and Swanson L 2003 *High Resolution Focused Ion Beams: FIB and its Application* (New York: Kluwer Academic Plenum)
[16] For a review see Nogués J and Schuller I K 1999 *J. Magn. Magn. Mater.* **192** 203
[17] Meiklejohn W P and Bean C P 1956 *Phys. Rev.* **102** 1413
[18] Meiklejohn W P and Bean C P 1957 *Phys. Rev.* **105** 904
[19] For a review see Nogués J, Sort J, Langlais V, Skumryev V, Suriñach S, Muñoz J S and Baró M D 2005 *Phys. Rep.* **422** 65
[20] For a theoretical review see Kiwi M 2001 *J. Magn. Magn. Mater.* **234** 584
[21] For a review see Iglesias O, Labarta A and Batlle X 2008 *J. Nanosci. Nanotechnol.* **8** 2761
[22] Roshchin I V, Petracic O, Morales R, Li Z P, Batlle X and Schuller I K 2005 *Europhys. Lett.* **71** 297
[23] Petracic O, Li Z-P, Roshchin I V, Viret M, Morales R, Batlle X and Schuller I K 2005 *Appl. Phys. Lett.* **87** 222509
[24] Roy S *et al* 2005 *Phys. Rev. Lett.* **95** 047201
[25] Li Z-P, Petracic O, Morales R, Olamit J, Batlle X, Liu K and Schuller I K 2006 *Phys. Rev. Lett.* **96** 217205
[26] Fitzsimmons M R, Kirby B J, Roy S, Li Z-P, Roshchin I V, Sinha S K and Schuller I K 2007 *Phys. Rev.* B **75** 214412
[27] Morales R, Li Z-P, Olamit J, Liu K, Alameda J M and Schuller I K 2009 *Phys. Rev. Lett.* **102** 097201
[28] Li Z-P, Morales R and Schuller I K 2009 *Appl. Phys. Lett.* **94** 142503
[29] Kovylina M, Erekhinsky M, Morales R, Villegas J E, Schuller I K, Labarta A and Batlle X 2009 *Appl. Phys. Lett.* **95** 152507
[30] Roshchin I V, Petracic O, Morales R, Li Z-P, Batlle X and Schuller I K *International Patent* PCT/US2005/025129
[31] Nogués J, Lederman D, Moran T J and Schuller I K 1996 *Phys. Rev. Lett.* **76** 4624